A Ketimide-Stabilized Palladium Nanocluster With a Hexagonal Aromatic Pd$_7$ Core

Andrew W. Cook,[a] Peter Hrobárik,*[b] Peter L. Damon,[a] Guang Wu,[a] and Trevor W. Hayton*[a]

[a] Department of Chemistry and Biochemistry, University of California Santa Barbara, Santa Barbara, CA 93106, USA

[b] Department of Inorganic Chemistry, Faculty of Natural Sciences, Comenius University, SK-84215 Bratislava, Slovakia

Abstract

Herein, we report the synthesis and characterization of the mixed-valent, ketimide-stabilized Pd_7 nanosheet, $[Pd_7(N=C^tBu_2)_6]$ (**1**), via reaction of $PdCl_2(PhCN)_2$ and $Li(N=C^tBu_2)$. Also formed in the reaction is ^tBuCN, isobutylene, and isobutane. The presence of these products suggests that $Li(N=C^tBu_2)$ acts as a reducing agent in the transformation, converting the Pd(II) starting material into the mixed-valent Pd(I)/Pd(0) product. Complex **1** features a hexagonal planar $[Pd_7]^{6+}$ core stabilized by six ketimide ligands, which surround the $[Pd_7]^{6+}$ center in an alternating up/down fashion. *In situ* NMR spectroscopic studies, as well as DFT calculations, suggest that **1** is formed via the intermediacy of bimetallic Pd(II) ketimide complex, $[(^tBu_2C=N)Pd(\mu-N,C-N=C(^tBu)C(Me)_2CH_2)Pd(N=C^tBu_2)]$ (**2**). DFT calculations also reveal that **1** is a rare example of an all-metal aromatic nanocluster with hexagonal symmetry, sustaining a net diatropic ring-current of 10.6 nA/T, which is similar to that of benzene (11.8 nA/T) or other well-established transition metal aromatic systems. Finally, we have found that **1** reacts with Ph_3P, cleanly forming the Pd(0) phosphine complex, $Pd(PPh_3)_3$ (**3**), suggesting that **1** could be a useful pre-catalyst for a variety of cross-coupling reactions.

Introduction

Atomically precise nanoclusters (APNCs) are attracting attention for their use in a variety of applications, including quantum computing,[1-3] catalysis,[4-6] and imaging.[7,8] While most attention has been paid to Ag- and Au-containing nanoclusters in the past few years,[9-11] the synthesis of Pd- and Pt-containing nanoclusters has been historically important to the APNC field.[12-14] These clusters typically feature a mixture of CO and PR_3 as stabilizing ligands, and can achieve large nuclearities.[15] Notable examples include $[Pd_4(CO)_4(OAc)_4]$,[16] $[Pd_{10}(CO)_{12}(P^nBu_3)_6]$,[17] $[Pd_{23}(CO)_{20}(PEt_3)_{10}]$,[18] and $[Pt_xPd_{164-x}(CO)_{72}(PPh_3)_{20}]$ ($x = 8$).[19] In these cases, the electron rich, low-valent M(0) core is likely stabilized by the presence of the π-accepting CO and PR_3 ligands. More recently, several low-valent Pd nanoclusters that do not contain CO or phosphine co-ligands have also been reported,[20] such as $[Pd_3(\mu_3\text{-}C_7H_7)_2]^{2+}$,[21] $[Pd_{13}(\mu_4\text{-}C_7H_7)_6]^{2+}$,[20,22] and $[Pd_6(\mu\text{-}GePh_2)_2(CN\text{-}2,6\text{-}Me_2C_6H_3)_8(\mu\text{-}CN\text{-}2,6\text{-}Me_2C_6H_3)_2]$.[23] Other noteworthy Pd nanoclusters include the Pd_{11} nanosheet, $[Pd_{11}(Si^iPr)_2(Si^iPr_2)_4(CN^tBu)_{10}]$,[24,25] the Pd_5 nanosheet, $[Pd_5(C_{18}H_{12})_2]^{2-}$,[21] and the Pd_6 "bow-tie" cluster, $[Pd_6Cl_2(SiPh_2)_2(CN^tBu)_8]$.[26] While these complexes do not contain CO or PR_3, in many case they still contain π-accepting ligands, such as isocyanides,[27] $[C_7H_7]^+$,[22] and silylenes.[28,29] That said, Pd nanoclusters are still relatively rare and only handful of ligands are known to stabilize this class of materials.

In an effort to address the synthetic challenge of preparing Pd nanoclusters, we have been searching for new ligands that can stabilize low-valent Pd. In this regard, the ketimide ligand ($R_2C=N^-$) appears to be a suitable choice. The ketimide ligand is known to be a good π-acceptor,[30,31] and thus should be able to stabilize low-valent metal clusters. Moreover, it is known to promote metal-metal bonding, as evidenced by the isolation of the bimetallic

complexes [Li(12-crown-4)$_2$][M$_2$(N=C^{t}Bu$_2$)$_5$] (M = Mn, Fe, Co),[32] each of which contains a strong M-M interaction. Ketimide ligands have also found use in the stabilization of high oxidation states, as well, as shown by the isolation of [M(N=C^{t}Bu$_2$)$_4$] (M = V, Nb, Ta, Cr, Mo, W, Mn, Fe, Co).[30,31,33-36] Moreover, ketimides are useful co-ligands for olefin polymerization catalysts,[37-39,40,41] and they can serve as "masked" nitrenes,[42] which can mediate C-H bond activation chemistry when unmasked. They have also appeared as intermediates in C-N bond forming reactions.[43,44] Yet, despite these diverse roles, ketimides have not been previously used to stabilize APNCs.

Herein, we report the synthesis and characterization of the ketimide-stabilized Pd$_7$ nanosheet, [Pd$_7$(N=C^{t}Bu$_2$)$_6$], demonstrating for the first time that ketimides can promote the formation of low-valent palladium APNCs.

Results and Discussion

Reaction of PdCl$_2$(PhCN)$_2$ with 2 equiv of Li(N=C^{t}Bu$_2$) in THF results in the formation of a dark green solution. Work-up of the reaction mixture results in the isolation of [Pd$_7$(N=C^{t}Bu$_2$)$_6$] (**1**), in 40% yield as deep green blocks (Scheme 1). Complex **1** is soluble in pentane, hexanes, Et$_2$O, benzene, toluene, and THF, and somewhat soluble in MeCN, but quickly decomposes in the presence of CH$_2$Cl$_2$. It is stable as a solid under inert atmosphere at -25 °C for at least several months. For comparison, reaction of PtCl$_2$(1,5-COD) with 2 equiv of Li(N=C^{t}Bu$_2$) results in formation of a mixture of the linear, two-coordinate Pt(II) complex, [Pt(N=C^{t}Bu$_2$)$_2$], and the bimetallic Pt(II) complex, [(^{t}Bu$_2$C=N)Pt(μ-N,C-N=C(^{t}Bu)C(Me)$_2$CH$_2$)-Pt(N=C^{t}Bu$_2$)].[45] No evidence is observed for the formation of the analogous Pt$_7$ nanosheet, [Pt$_7$(N=C^{t}Bu$_2$)$_6$], in that reaction (see further discussion below).
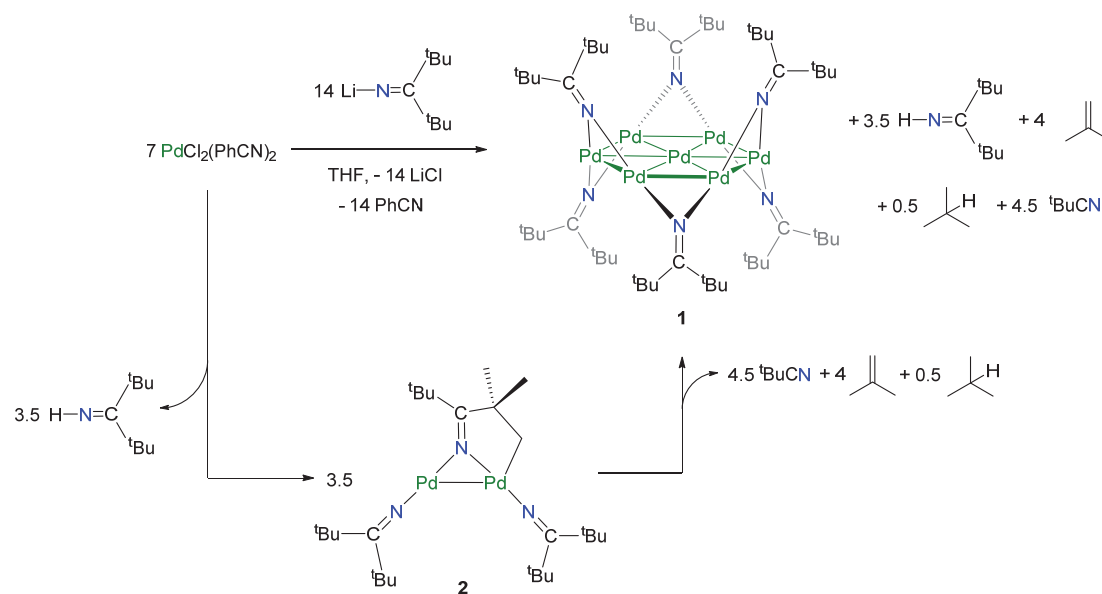
Scheme 1. Synthesis of the palladium nanosheet Pd$_7$(N=C^{t}Bu$_2$)$_6$ (**1**)

Complex **1** crystallizes in the triclinic space group *P*-1. Its planar [Pd$_7$]$^{6+}$ core lies upon a center of inversion and consists of a hexagonal arrangement of six Pd atoms (Figure 1). A seventh Pd atom resides at the center of the hexagon and features a hexagonal planar coordination geometry. All seven Pd atoms are co-planar. Each ketimide ligand bridges two outer, adjacent Pd atoms in an alternating up/down fashion. As a result, the complex has overall D$_{3d}$ symmetry. The Pd-Pd bond distances fall within a narrow range (2.7024(5) to 2.7159(6) Å), and are within the range of those reported for Pd-Pd single bonds.[46] The average Pd-N bond length is 2.00 Å, which is comparable to the Pd-N bond lengths reported for the terminal Pd(II) ketimides, [Pd(PCy$_3$)$_2$(O$_2$CC$_6$F$_5$)(N=CRR')] (1.956(3) Å for RR' = C$_{10}$H$_{10}$; and 1.999(3) Å for RR' = Me{CHPh$_2$}),[44,47] as well as terminal Pd(II) amides.[48,49] Finally, the average N-Pd-N angle is 172°, highlighting the fact that the coordination geometry about the outer Pd ions is nearly linear if the Pd-Pd bonds are ignored.
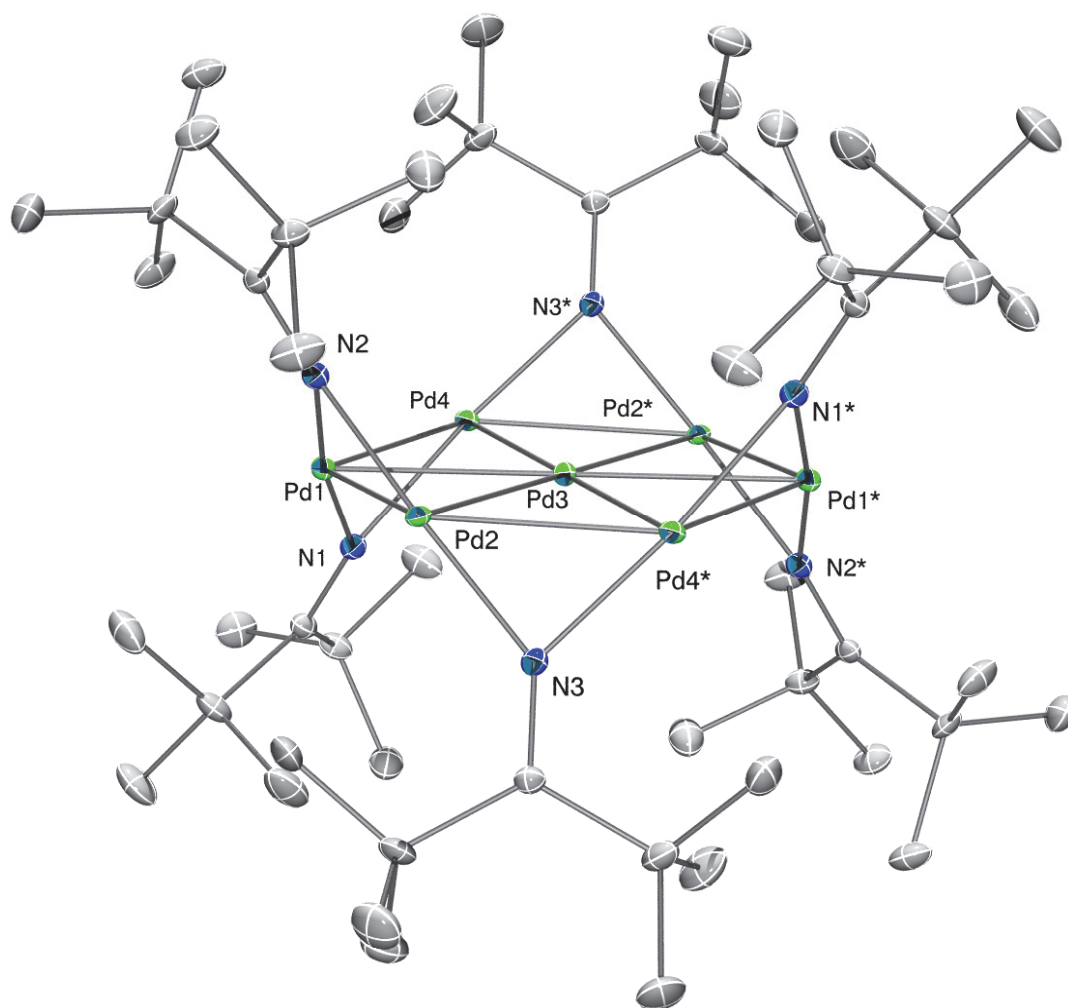
Figure 1. ORTEP diagram of **1**. Hydrogen atoms are omitted for clarity. Selected bond distances (Å) and angles (°): Pd1-N1 = 1.990(6), Pd1-N2 = 1.995(6), Pd2-N3 = 1.986(8), Pd2-N1 = 2.015(8), Pd4-N2 = 2.003(4), Pd4-N3 = 2.005(4), Pd1-Pd3 = 2.7024(5), Pd1-Pd4 = 2.7128(8), Pd1-Pd2 = 2.7137(11), Pd2-Pd4 = 2.7018(6), Pd2-Pd3 = 2.7159(6), Pd3-Pd4 = 2.7079(8), avg. N-Pd-N = 172.

The hexagonal planar coordination geometry is relatively rare. Tanase and co-workers recently reported [Pt{Pd(dmpe)}$_3$(μ_3-SiPh$_2$)$_3$], wherein the Pt atom is ligated by a hexagonal array of

three Pd atoms and three Si atoms,[50] while Crimmin and co-workers recently reported the hexagonal planar Pd complex, $[PdH_3(MgL^{Me})_3]$ (L^{Me} = {(2,6-^{i}Pr$_2$C$_6$H$_3$)NC(Me)}$_2$CH).[51] Also of note is [Ni(*cyclo*-P^{t}Bu)$_6$], which contains a hexagonal planar Ni center,[52] $[Mn_7(THF)_6(CO)_{12}]^-$, which contains a hexagonal planar Mn center,[53] and $[M_5Fe_4(CO)_{16}]^{3-}$ (M = Cu, Ag), which contains a hexagonal planar group 11 ion.[54,55] The clusters $[Co_7H_6\{N(SiMe_3)_2\}_6]$, $Pd[Re_2(CO)_8(\mu\text{-}SbPh_2)(\mu\text{-}H)]_2$, and $[Rh_7H_{18}(P^iPr_3)_6]^{2+}$ contain comparable hexagonal planar $[M_7]$ cores,[56-58] but the central metal ions in these structures are also bridged by μ_3-hydride ligands.

The ^{1}H NMR spectrum of **1** in C$_6$D$_6$ features a sharp singlet at 1.65 ppm (Figure S1), consistent with the high-symmetry observed in the solid-state. The ^{13}C{^{1}H} NMR spectrum displays a diagnostic resonance at 181.0 ppm (Figure S2 in SI), assignable to the ketimide N=C carbon. A similar chemical shift (188.5 ppm) was observed for the copper ketimide cluster, $[Cu(N=C^tBu_2)]_4$.[59] The ESI mass spectrum of **1** features a signal at *m/z* 1586.2362 (Figure 2), corresponding to the parent $[M]^+$ ion (calcd *m/z* 1586.1953). A second prominent peak at *m/z* 740.1635 is assigned to the fragmentation product, $[Pd_3(N=C^tBu_2)_3]^+$ (calcd *m/z* 740.1459). The presence (or absence) of hydride ligands in transition metal nanoclusters is sometimes difficult to ascertain, as shown by the recent re-characterization of [Ag$_{40}$(S-2,4-Me$_2$C$_6$H$_3$)$_{24}$(PPh$_3$)$_8$H$_{12}$]$^{2+}$.[60,61] However, in this case, the excellent agreement between the observed and calculated isotope distributions for both signals (Figures S8 and S9) supports the absence of bridging hydride ligands in this complex.
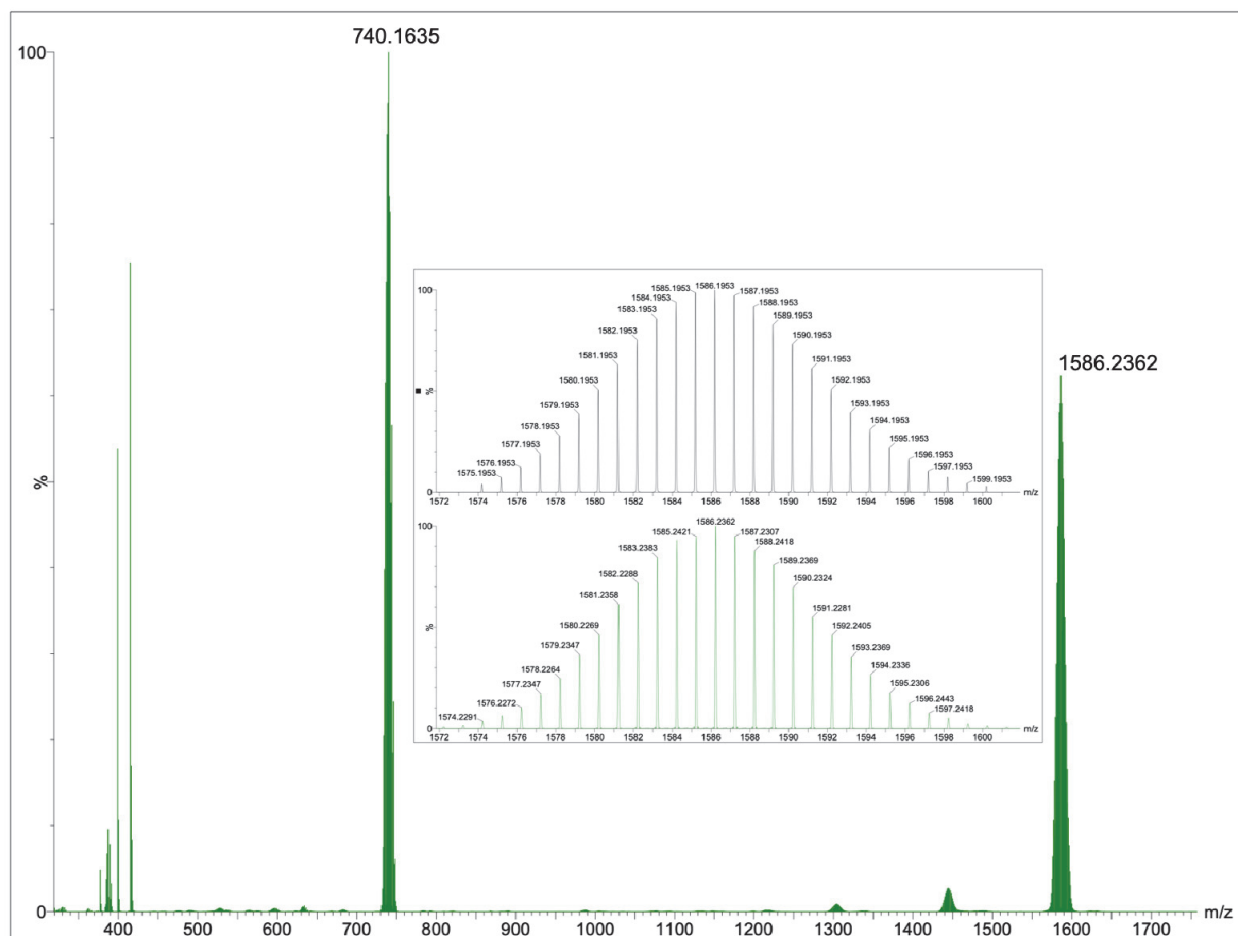
Figure 2. ESI-MS of $Pd_7(N=C^tBu_2)_6$ (**1**) in THF. The peak at *m/z* 1586.2362 denotes the peak assignable to the $[M]^+$ ion, whereas the peak at *m/z* 740.1635 denotes the peak assignable to the $[Pd_3(N=C^tBu_2)_3]^+$ fragment. Inset: experimental (bottom) and calculated (top) peaks assignable to the $[M]^+$ ion.

To better understand the formation of **1**, and identify the overall stoichiometry of the transformation, we recorded a ^1H NMR spectrum of the reaction mixture in THF-d_8, in the presence of an internal standard (Figures S3 and S4). This spectrum reveals the presence of resonances assignable to **1**, $HN=C^tBu_2$, ^tBuCN, isobutylene, and isobutane. Also present are resonances at 2.38, 1.66, 1.60, and 1.54, 1.30, 1.24, and 1.18 ppm, which we have assigned to

[(^{t}Bu$_2$C=N)Pd(μ-N,C-*N*=C(^{t}Bu)C(Me)$_2$*C*H$_2$)Pd(N=C^{t}Bu$_2$)] (**2**) (Scheme 1 and Figure 3 for

comparison of structures of analogous Pd and Pt complexes). This complex is the Pd analogue

of the recently reported bimetallic Pt ketimide, [(^{t}Bu$_2$C=N)Pt(μ-N,C-

N=C(^{t}Bu)C(Me)$_2$*C*H$_2$)Pt(N=C^{t}Bu$_2$)].[45] These resonances are observed in a 2:9:9:9:6:9:9 ratio.

Both the chemical shifts and relative intensities are essentially identical to those observed for the

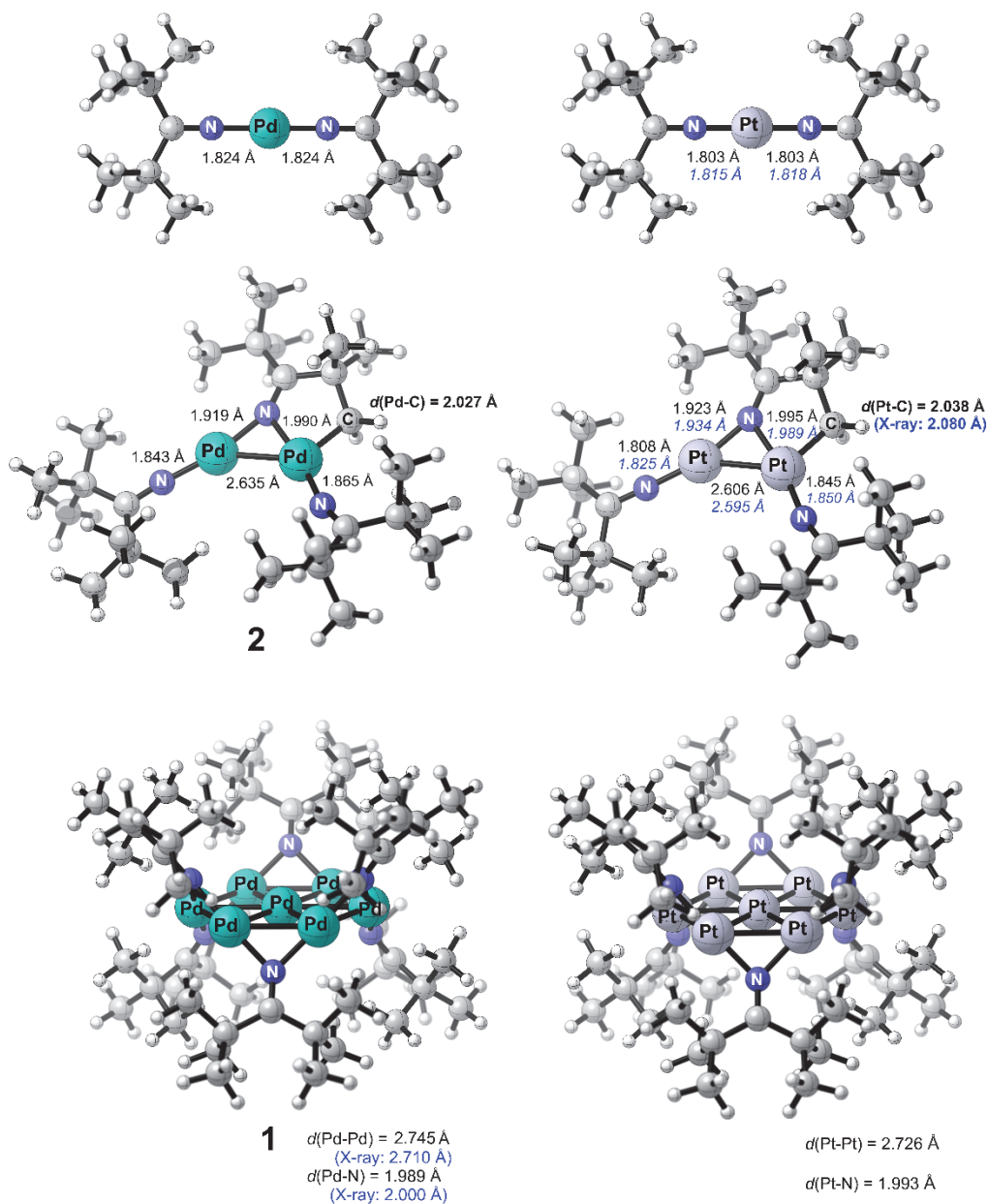Pt analogue, supporting our assignment.

9

Figure 3. Comparison of DFT (PBE0-D3(BJ)/ECP/def2-TZVP) optimized structures and pertinent bond-lengths in analogous Pd and Pt ketimide complexes, $M(N=C^tBu_2)_2$, $[(^tBu_2C=N)Pt(\mu\text{-}N,C\text{-}NC(^tBu)C(Me)_2CH_2)Pt(N=C^tBu_2)]$ and $M_7(N=C^tBu_2)_6$ (M = Pd, Pt). Experimentally determined bond lengths are indicated in blue.

Given the distribution of products in the reaction mixture, we hypothesize that the formation of **1** proceeds via the intermediacy of **2**. Specifically, we propose that reaction of $PdCl_2(PhCN)_2$ with $Li(N=C^tBu_2)$ results in initial formation of **2** and $HN=C^tBu_2$. Complex **2** then converts to low-valent **1** via oxidation of its ketimide ligands, concomitant with formation of ^tBuCN, isobutylene, and isobutane (Scheme 1). *In situ* NMR spectroscopic monitoring appears to confirm this hypothesis (Figure S5). Thermochemical calculations at the DFT level are also consistent with this proposal, as the formation of $Pd_7(N=C^tBu_2)_6$ (**1**) from $[(^tBu_2C=N)Pd(\mu\text{-}N,C\text{-}N=C(^tBu)C(Me)_2CH_2)Pd(N=C^tBu_2)]$ (**2**) was found to be highly exergonic (Scheme 2). Moreover, we have previously demonstrated that thermolysis of $M(N=C^tBu_2)_4$ (M = Mn, Fe) results in ketimide oxidation and formation of $Mn_3(N=C^tBu_2)_6$ and $Fe_2(N=C^tBu_2)_5$, respectively, along with ^tBuCN, isobutane, and isobutylene.[34,35] Incidentally, our calculations also explain why the Pt analogue of **1**, $[Pt_7(N=C^tBu_2)_6]$, is not experimentally observed during the reaction of $PtCl_2(1,5\text{-}COD)$ with $Li(N=C^tBu_2)$.[45] Its formation from the $[(^tBu_2C=N)Pt(\mu\text{-}N,C\text{-}N=C(^tBu)C(Me)_2CH_2)Pt(N=C^tBu_2)]$ intermediate is actually slightly endergonic due to large positive reaction enthalpy associated with higher bond-breaking costs of the more covalent Pt-N/Pt-C bonds in comparison to their Pd-L counterparts.[45]
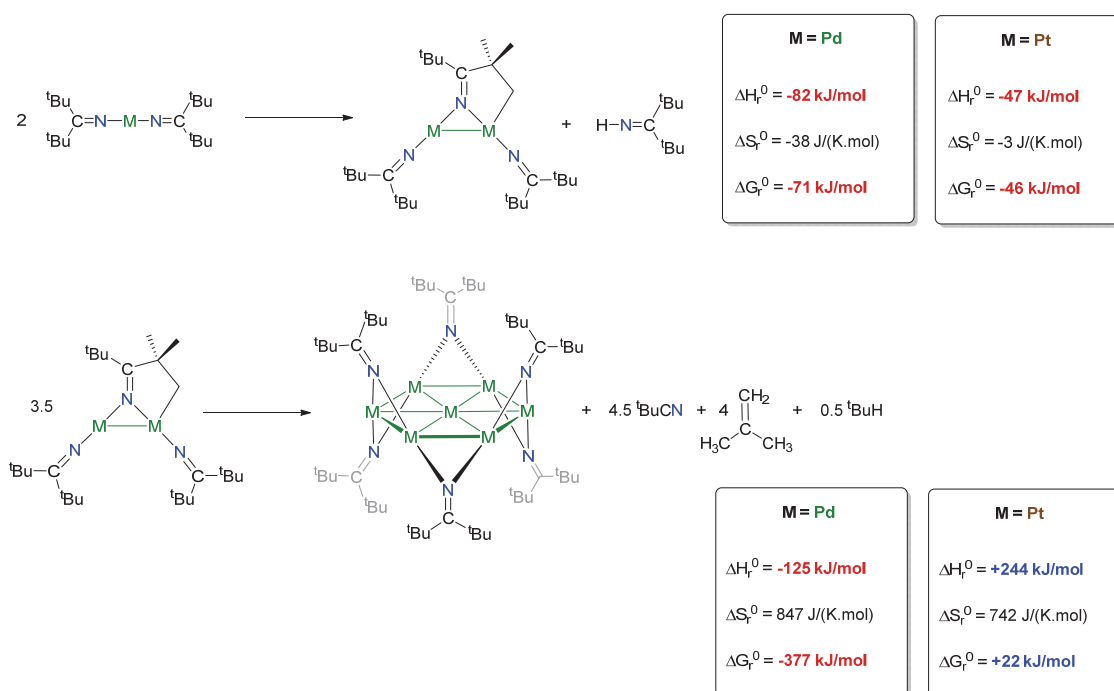
Scheme 2. Computed reaction enthalpies (ΔH_r^0), entropies (ΔS_r^0) and free Gibbs energies (ΔG_r^0) for selected transformations of analogous Pd and Pt ketimide complexes (PBE-D3(BJ)/def2-TZVPP results in gas-phase).

In an effort to understand the unique structural features of complex **1**, we performed a computational bonding analysis using quasi-relativistic DFT calculations at the PBE0-D3(BJ)/ECP/def2-TZVP level of theory. Calculations were performed on **1**, as well as the truncated model complexes, $Pd_7(N=CMe_2)_6$ and $Pd_7(N=CH_2)_6$. These calculations reveal a rich manifold of Pd-Pd bonding interactions (see Figures 4 and S16 for canonical MOs and Figure S17 for ELF analysis). For example, the HOMO and HOMO-1 for $Pd_7(N=CH_2)_6$ are highly delocalized and predominately Pd-based (Figure 4). Similar results have been found for other Pd nanoclusters.[20,23]

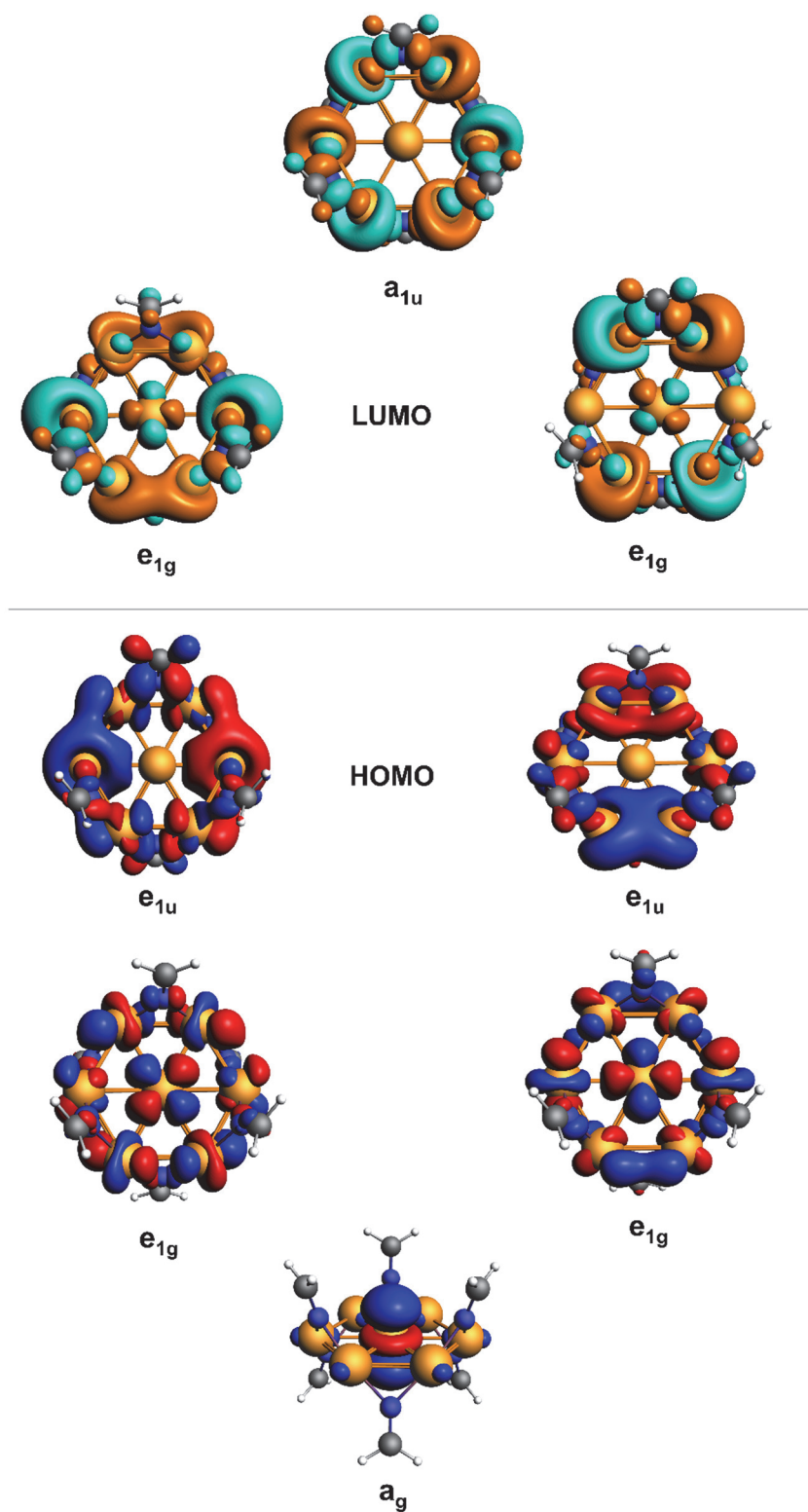**Figure 4.** Frontier MOs (isosurface plots ±0.03 au) in $Pd_7(N=CH_2)_6$ (a truncated model complex of **1**).

The calculated NPA atomic charges for the outer and inner Pd atoms of **1** are +0.41 and +0.08, respectively, consistent with their formal oxidations states of +1 and 0. Neither the ligand-free $[Pd_6]^{6+}$ nor $[Pd_7]^{6+}$ cores are stable alone (no stationary points on the potential energy surface were found), and both require anionic bridging ligands to hold the outer, positively charged Pd atoms together. We note further that dispersion forces play only a minor role in the overall stability of the neutral $Pd_7(N=C^tBu_2)_6$ cluster (the Pd-Pd bonds are elongated only by 0.015 Å when optimizing the structure without Grimme's D3(BJ) dispersion corrections; cf. Table S3 in Supporting Information), and the central Pd(0) atom features a strong bonding energy (375 kJ/mol) to the outer hexagonal $[Pd_6]$ ring, as revealed from energy decomposition analysis (EDA). Interestingly, the structures of both the $[Pd_7]$ and $[Pd_6]$ cores remain planar and Pd-Pd distances are almost unaffected upon replacing the bridging ketimide ligands with other monoanionic π-donors, such as halides, thiocyanates, or alkylthiolates (Table 1), hinting at the extra stabilization energy (e.g., aromaticity) within the hexagonal ring. The presence of aromaticity was confirmed by the gauge-including magnetically induced current (GIMIC) method,[62,63] which was used to evaluate ring currents and visualize current densities in the $[Pd_nL_6]$ clusters in comparison with other widely recognized aromatics (cf. Table 1 as well as Table S4 and Figure S14 together with a short discussion in Supporting Information). Hence, complex **1** sustains a net diatropic ring-current of 10.6 nA/T (see also Figure 5 for the current density), which is comparable with that of benzene (11.8 nA/T) and other well-established transition metal aromatics, such as $[Mo_3O_9]^{2-}$ (11.1 nA/T) and $[(Ar_3P)_3Pd_3(SR)_3]^+$ (14.8 nA/T), the latter being noble-metal analogues of the cyclopropenium ion.[64-66] In addition, the computed vertical electron detachment energy (VDE) for **1** is relatively high (5.30 eV) and comparable with that of $[Mo_3O_9]^-$ (4.0 eV).[65]

Table 1. Computed Pd-Pd distances and ring-current strengths in selected [Pd_n] (n = 7, 6, 3) clusters, [Mo_3O_9]$^{2-}$, and benzene

	d(Pd-Pd) [Å]	ring-current strength [nA/T] [b]		
		diatropic	paratropic	net
Pd7(**N**=C^{t}Bu2)6 (**1**)	2.745	21.8	-11.2	10.6
Pd7(**N**=CMe2)6	2.718	16.3	-4.4	11.9
Pd7(**N**=CH2)6	2.721	15.9	-3.9	12.0
Pd7(**S**CN)6	2.724	16.9	-8.4	8.5
Pd7(**S**Me)6	2.713	16.3	-8.2	8.1
Pd7**F**6	2.720	13.6	-4.9	8.7
Pd7**Cl**6	2.720	16.9	-7.7	9.2
Pd7**Br**6	2.714	17.8	-7.1	10.7
Pd7**I**6	2.717	22.8	-8.4	14.4
Pd6(**N**=CMe2)6	2.681	15.6	-6.5	9.1
[(H3**P**)3Pd3(**S**H)3]$^+$	2.859	15.2	-0.4	14.8
[Mo3**O**9]$^{2-}$ (D_{3h})	-	11.5	-0.4	11.1
C6**H**6	-	16.8	-5.0	11.8

[a] Structures optimized at the PBE0-D3(BJ)/ECP/def2-TZVP level. [b] The integrated current passing outer ring (B3LYP-D3(BJ)/TZVPP results; cf. Computational details). An integration plane is placed into the geometrical ring center or into the center of Pd3 triangles in the case of [Pd7] clusters, so that the integration plane is perpendicular to the planar ring and it passes through the center of M-L bonds (ligating atoms are indicated in bold). See also Table S4 in Supporting Information for more details and calculated nuclear independent chemical shift (NICS) values.
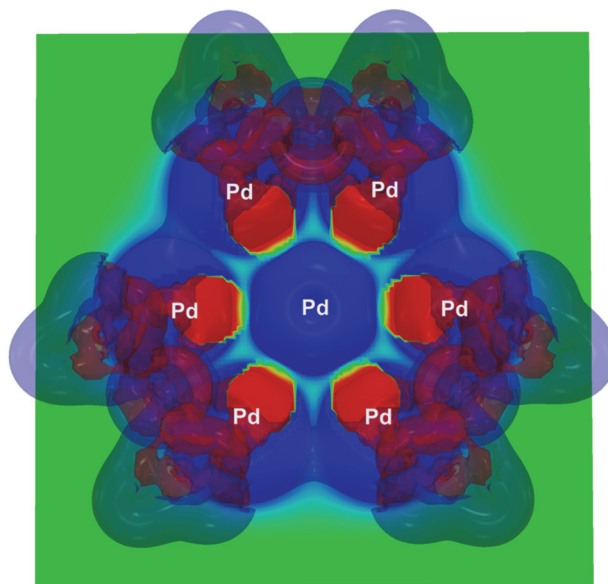
Figure 5. Signed modulus of the current density in $Pd_7(N=CH_2)_6$ (a truncated model of **1**). Cut-plane plot within the $[Pd_7]$ plane. Diatropic currents are illustrated in blue, paratropic currents are illustrated in red. For more details, see Supporting Information.

We also recorded the cyclic voltammogram of **1** in THF at a variety of scan rates. Most notably, complex **1** features a reversible reduction feature at $E_{1/2}$ = -2.32 V (vs. Fc/Fc^+) (Figures 6, S12 – S13 and Table S2). The reversibility of this feature suggests that **[1]$^-$** could be isolable. Additionally, we observe the presence of an irreversible oxidation feature at $E_{p,a}$ = -0.18 V (vs. Fc/Fc^+, 100 mV/s scan rate). This feature is irreversible at all scan rates studied. Interestingly, after scanning past -0.18 V, a new feature appears in the cyclic voltammogram, suggesting that the oxidation of **1** results in formation of a new species via an *ECE*-type mechanism. This new feature appears at -1.35 V (vs. Fc/Fc^+, 100 mV/s scan rate) and is irreversible at all scan rates studied. The identity of this new species is unknown. For comparison, the Pd_{13} nanocluster $[Pd_{13}Tr_6]^{2+}$ features a reversible reduction feature at -1.08 V and reversible oxidation features at +0.05 V and +0.73 V (vs. Fc/Fc^+).[20] The Pd_6 nanocluster, $[Pd_6(\mu\text{-}GePh_2)_2\text{-}(CN\text{-}2,6\text{-}$

Me$_2$C$_6$H$_3$)$_8$(μ-CN-2,6-Me$_2$C$_6$H$_3$)$_2$], also exhibits rich electrochemistry, including reversible redox features at ca. -1.35 V and -1.03 V (vs. Fc/Fc$^+$).[23] While quantitative comparisons are a challenge because of their different nuclearities and ligands sets, it is clear that reversible addition or removal of electrons to the Pd bonding framework is a common trait amongst Pd nanoclusters.
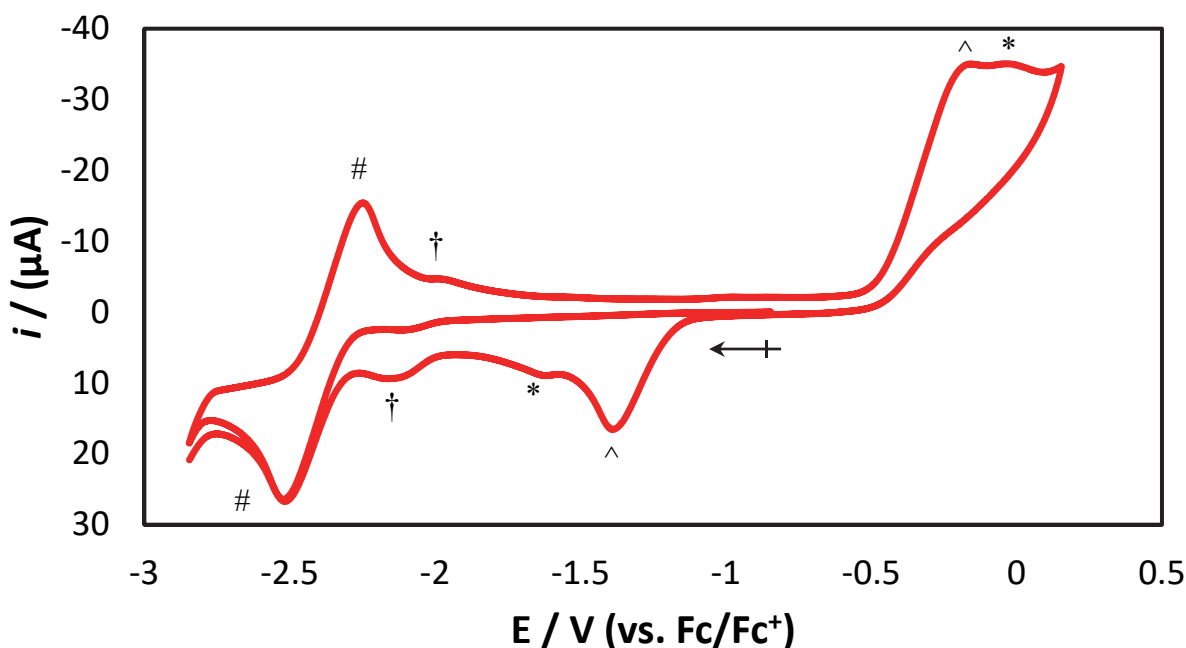
Figure 6. Cyclic voltammogram of complex **1** (200 mV/s, vs. Fc/Fc$^+$), measured in THF with 0.1 M [NBu$_4$][PF$_6$] as supporting electrolyte. The electrochemical feature indicated by (#) is assigned to the [**1**]$^{0/-}$ couple; the electrochemical feature indicated by (^) is due to the irreversible oxidation of **1** via an *ECE*-type mechanism, which gives rise to the reduction at -1.4 V; the electrochemical features indicated by (*) are likely due to a decomposition product, as they grow in intensity during the course of the experiment; the electrochemical feature indicated by (†) is ascribed to a trace amount of **2**.

Finally, we undertook a preliminary reactivity study of complex **1**. Addition of 21 equiv of

PPh₃ to **1** in THF resulted is a slow color change from deep forest green to pale green over the

course of 48 h at room temperature (Scheme 3). Work-up of the reaction mixture resulted in the

isolation of Pd(PPh₃)₃ (**3**) as yellow blocks in 82% yield. The ^{1}H and ^{31}P{^{1}H} NMR spectra of **3**

in C₆D₆ match closely to those previously reported for this material in toluene-d_8 (Figures S6 and

S7).[67,68] To account for the reduction of the Pd centers in **1** upon formation of **3**, we propose the

ketimide ligands are oxidized, forming ^{t}BuCN, isobutane, and isobutylene as by-products. A

similar process is occurring during the initial formation of **1** and further demonstrates the redox

activity of the ketimide ligand. Significantly, the facile formation of Pd(0) upon decomposition

of **1** suggests that it could be a useful catalyst precursor for a variety of cross coupling

reactions.[69-71] Indeed, Pd nanoclusters and nanoparticles have previously been shown to act as

reservoirs for catalytically-competent mono-metallic Pd(0) species.[72]
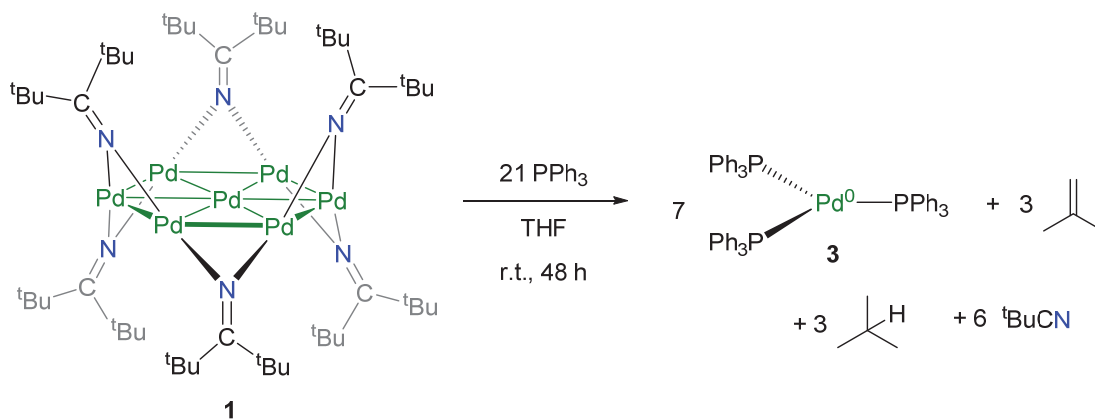
Scheme 3. Synthesis of Pd(PPh₃)₃ (**3**).

Conclusions

The isolation of the Pd₇ nanosheet, Pd₇(N=C^{t}Bu₂)₆ (**1**), via reaction of PdCl₂(PhCN)₂ and

Li(N=C^{t}Bu₂), demonstrates that ketimides are effective at stabilizing low-valent group 10

nanoclusters, thereby broadening the scope of ligands that are known to promote the formation of this class of materials. Complex **1** is built around a $[Pd_7]^{6+}$ core and its central Pd atom features a rare hexagonal planar coordination geometry. According to DFT calculations, **1** features a similar level of aromaticity as other previously reported 4d transition metal aromatic clusters, such as $[Mo_3O_9]^{2-}$ or $[(Ar_3P)_3Pd_3(SR)_3]^+$, but **1** is unique because it is the first all-metal system with hexagonal (i.e., benzene-like) symmetry. Preliminary reactivity studies suggest that **1** can act as a source of Pd(0), a consequence of the facile oxidative decomposition of the ketimide ligands. Going forward, we plan to explore the small molecule reactivity of $Pd_7(N=C^tBu_2)_6$, which, given the unique coordination environment of the central Pd(0) atom, could result in new modes of reactivity. In addition, we will explore the ability of the ketimide ligand to stabilize higher nuclearity Pd clusters, which could potentially be achieved by changing the alkyl substituents on the ketimide ligand.

Experimental

General Procedures. All reactions and subsequent manipulations were performed under anaerobic and anhydrous conditions in the glovebox under an atmosphere of dinitrogen. Hexanes, diethyl ether (Et$_2$O), and tetrahydrofuran (THF) were dried by passage over activated molecular sieves using a Vacuum Atmospheres DRI-SOLV solvent purification system. Pentane, dichloromethane, and benzene were dried on an MBraun solvent purification system. Isooctane and acetonitrile were degassed and stored over activated 3 Å molecular sieves for 72 h prior to use. C$_6$D$_6$, THF-d_8, and hexamethyldisiloxane (HMDSO) were dried over activated 3 Å molecular sieves for 24 h prior to use. Li(N=C^{t}Bu$_2$)[73] and PdCl$_2$(PhCN)$_2$[74] were prepared by literature procedures. All other reagents were purchased from commercial suppliers and used as received.

^{1}H and ^{13}C{^{1}H} NMR spectra were recorded on an Agilent Technologies 400-MR DD2 400 MHz spectrometer or Varian Unity Inova 500 MHz spectrometer at 25 ºC. The chemical shifts of ^{1}H and ^{13}C nuclei were referenced by using the residual solvent peaks (^{1}H NMR experiments) or the characteristic resonances of the solvent nuclei as internal standards (^{13}C{^{1}H} NMR experiments).

IR spectra were recorded on a Nicolet 6700 FT-IR spectrometer. UV-Vis/NIR spectra were recorded on a Shimadzu UV3600 UV-NIR spectrometer. Mass spectra were collected by the Mass Spectrometry Facility at the University of California, Santa Barbara, using an electrospray ion (ESI) source on positive ion mode with a Waters Micromass QTOF2 Quadrupole/Time-of-Flight Tandem mass spectrometer. Elemental analyses were performed by the Microanalytical Laboratory at University of California (Berkeley, CA).

Cyclic Voltammetry Measurements. CV experiments were performed with a CH Instruments 600c Potentiostat, and the data were processed using CHI software (version 6.29). All experiments were performed in a glove box using a 20 mL glass vial as the cell. The working electrode consisted of a platinum disk embedded in glass (2 mm diameter), the counter electrode was a Pt wire, and the reference electrode was a Pt wire. Solutions employed during CV studies were typically 1 mM in complex **1** and 0.1 M in [Bu$_4$N][PF$_6$]. All potentials are reported versus the [Cp$_2$Fe]$^{0/+}$ couple. For all trials, $i_{p,a}/i_{p,c}$ = 1 for the [Cp$_2$Fe]$^{0/+}$ couple, while $i_{p,c}$ increased linearly with the square root of the scan rate (i.e., $\sqrt{v}$). Redox couples which exhibited behavior similar to the [Cp$_2$Fe]$^{0/+}$ couple were considered reversible.

Synthesis of Pd$_7$(N=C^{t}Bu$_2$)$_6$ (1): In a 20 mL scintillation vial equipped with a magnetic stir bar, PdCl$_2$(PhCN)$_2$ (107 mg, 0.28 mmol) was dissolved in THF (2 mL) to give an orange solution, which was subsequently cooled to -25 ºC. Concurrently, 2 equiv of Li(N=C^{t}Bu$_2$) (82 mg, 0.56

mmol) was dissolved in THF (2 mL) to give a colorless solution, which was also cooled to -25 ºC. Over the course of 1 min, the Li(N=C^{t}Bu$_2$) solution was added dropwise to a stirring solution of PdCl$_2$(PhCN)$_2$. The reaction mixture was then allowed to warm to room temeprature with sitrring. The resulting mixture slowly turned to a dark forest green color. After 5h, the volatiles were removed *in vacuo* to give a dark green oily solid. This solid was dissolved in pentane (2 mL) and filtered through a Celite column supported on glass wool (0.5 cm × 2 cm) to give a clear dark green filtrate, while leaving a white precipitate on the Celite. The filter pad was washed with pentane (2 × 1 mL) and added to the filtrate. The filtrate (in a 5 mL vial) was placed inside of a 20 mL scintillation vial containing 4 mL of isooctane. Storage of this two-vial system at -25 °C for 7 d resulted in the deposition of dark green blocks of **1**, which were isolated by decanting the supernatant (26 mg, 40% yield). The ^{1}H NMR data for this sample also reveals the presence of a small amount of [(^{t}Bu$_2$C=N)Pd(μ-N,C-*N*=C(^{t}Bu)C(Me)$_2$*CH$_2$*)Pd(N=C^{t}Bu$_2$)] (**2**). Complexes **1** and **2** were present in a 6:1 ratio. All attempts to isolate analytically pure **2** have thus far been unsuccessful. ^{1}H NMR (C$_6$D$_6$, 25°C, 400 MHz): δ 1.15 (**2**, s, 9H, C(C*H$_3$*)$_3$), 1.27 (**2**, s, 9H, C(C*H$_3$*)), 1.28 (**2**, s, 9H, C(C*H$_3$*)$_3$), 1.47 (**2**, s, 9H, C(C*H$_3$*)$_3$), 1.49 (**2**, s, 6H, C(C*H$_3$*)$_2$(CH$_2$)), 1.53 (**2**, s, 9H, C(C*H$_3$*)$_3$), 1.65 (**1**, s, 108H, C(C*H$_3$*)$_3$), 3.08 (**2**, s, 2H, C(CH$_3$)$_2$(C*H$_2$*)). ^{13}C{^{1}H} NMR (C$_6$D$_6$, 25 °C, 126 MHz): δ 32.97 (**1**, s, C(*CH$_3$*)$_3$), 42.83 (**1**, s, *C*(CH$_3$)$_3$), 180.97 (**1**, s, N=*C*). Anal. Calcd. for C$_{54}$H$_{108}$N$_6$Pd$_7$: C, 40.88; H, 6.86; N, 5.30. Found: C, 40.75; H, 6.66; N, 5.04. IR (KBr pellet, cm^{-1}): 3003 (m), 2946 (s), 2922 (s), 1579 (ν(C=N), s), 1566 (ν(C=N), s), 1477 (s), 1443 (s), 1383 (m), 1360 (s), 1260 (vw), 1214 (s), 1103 (w), 1042 (w), 973 (w), 925 (w), 840 (w), 688 (w), 668 (w). UV-Vis / NIR (pentane, 18.9 μM, 25 °C, L·mol^{-1}·cm^{-1}) 251 nm (ε = 99,900), 290 nm (sh, ε = 69,500), 369 nm (ε = 56,200), 420 nm (sh, ε = 33,400), 604 nm (ε = 17,100), 771 nm (ε = 16,300).

ESI-MS: m/z 1586.2362 [M]$^+$ (Calcd m/z 1586.1953), 740.1635 [Pd$_3$(N=C^{t}Bu$_2$)$_3$]$^+$ (Calcd m/z 740.1459).

Reaction of 1 with PPh$_3$: To a stirring, deep green solution of **1** (24 mg, 0.016 mmol) in THF (2 mL) was added PPh$_3$ (87 mg, 0.33 mmol) as a clear colorless THF solution (2 mL). The reaction mixture was stirred at room temperature for 48 h, whereupon the mixture lightened to pale green. The volatiles were removed in vacuo to give a pale green solid. The solid was rinsed with hexanes (2 mL) to afford a yellow solid. The solid was then dissolved in toluene (5 mL) and the resulting solution was filtered through a Celite column supported on glass wool (0.5 cm × 2 cm) to give a clear yellow filtrate. The filtrate was concentrated to ca. 2 mL and layered with hexanes (5 mL). Storage of this solution at -25 °C for 24 h resulted in the deposition of yellow blocks of Pd(PPh$_3$)$_3$ (**3**), which were isolated by decanting the supernatant (79 mg, 82%). The ^{1}H and ^{31}P NMR spectra of **3** were in good agreement with the reported spectra.[67]

ASSOCIATED CONTENT

- Experimental and computational details and additional data/analysis for complexes **1** and **2** (PDF)
- X-ray crystallographic details (CIF)
- Cartesian coordinates of the selected DFT-optimized structures (XYZ)

AUTHOR INFORMATION

Corresponding Authors

*hayton@chem.ucsb.edu

*peter.hrobarik@uniba.sk

ACKNOWLEDGMENT

REFERENCES

(1)   Long, D.-L.; Tsunashima, R.; Cronin, L. Polyoxometalates: Building Blocks for Functional Nanoscale Systems. *Angew. Chem. Int. Ed.* **2010**, *49*, 1736-1758.

(2)   Gaita-Ariño, A.; Luis, F.; Hill, S.; Coronado, E. Molecular spins for quantum computation. *Nat. Chem.* **2019**, *11*, 301-309.

(3)   Tejada, J.; Chudnovsky, E. M.; del Barco, E.; Hernandez, J. M.; Spiller, T. P. Magnetic qubits as hardware for quantum computers. *Nanotechnology* **2001**, *12*, 181.

(4)   Li, G.; Jin, R. Atomically Precise Gold Nanoclusters as New Model Catalysts. *Acc. Chem. Res.* **2013**, *46*, 1749-1758.

(5)   Liu, L.; Corma, A. Metal Catalysts for Heterogeneous Catalysis: From Single Atoms to Nanoclusters and Nanoparticles. *Chem. Rev.* **2018**, *118*, 4981-5079.

(6)   Cook, A. W.; Jones, Z. R.; Wu, G.; Scott, S. L.; Hayton, T. W. An Organometallic Cu_{20} Nanocluster: Synthesis, Characterization, Immobilization on Silica, and "Click" Chemistry. *J. Am. Chem. Soc.* **2018**, *140*, 394-400.

(7)   Chen, L.-Y.; Wang, C.-W.; Yuan, Z.; Chang, H.-T. Fluorescent Gold Nanoclusters: Recent Advances in Sensing and Imaging. *Anal. Chem.* **2015**, *87*, 216-229.

(8)   Colombo, M.; Carregal-Romero, S.; Casula, M. F.; Gutierrez, L.; Morales, M. P.; Bohm, I. B.; Heverhagen, J. T.; Prosperi, D.; Parak, W. J. Biological applications of magnetic nanoparticles. *Chem. Soc. Rev.* **2012**, *41*, 4306-4334.

(9)   Chakraborty, I.; Pradeep, T. Atomically Precise Clusters of Noble Metals: Emerging Link between Atoms and Nanoparticles. *Chem. Rev.* **2017**, *117*, 8208-8271.

(10)   Saillard, J.-Y.; Halet, J.-F. Structure and Bonding Patterns in Large Molecular Ligated Metal Clusters. *Struct. Bond.* **2016**, *169*, 157-179.

(11)   Jin, R.; Zeng, C.; Zhou, M.; Chen, Y. Atomically Precise Colloidal Metal Nanoclusters and Nanoparticles: Fundamentals and Opportunities. *Chem. Rev.* **2016**, *116*, 10346-10413.

(12)   Femoni, C.; Iapalucci, M. C.; Kaswalder, F.; Longoni, G.; Zacchini, S. The possible role of metal carbonyl clusters in nanoscience and nanotechnologies. *Coord. Chem. Rev.* **2006**, *250*, 1580-1604.

(13)   Mednikov, E. G.; Dahl, L. F. Syntheses, structures and properties of primarily nanosized homo/heterometallic palladium CO/PR_3-ligated clusters. *Philos. Trans. Royal Soc. A* **2010**, *368*, 1301-1332.

(14)   Zacchini, S. Using Metal Carbonyl Clusters To Develop a Molecular Approach towards Metal Nanoparticles. *Eur. J. Inorg. Chem.* **2011**, *2011*, 4125-4145.

(15)   Erickson, J. D.; Mednikov, E. G.; Ivanov, S. A.; Dahl, L. F. Isolation and Structural Characterization of a Mackay 55-Metal-Atom Two-Shell Icosahedron of Pseudo-Ih Symmetry, $Pd_{55}L_{12}(\mu_3\text{-}CO)_{20}$ (L = PR$_3$, R = Isopropyl): Comparative Analysis with Interior Two-Shell Icosahedral Geometries in Capped Three-Shell Pd_{145}, Pt-Centered Four-Shell Pd–Pt M_{165}, and Four-Shell Au_{133} Nanoclusters. *J. Am. Chem. Soc.* **2016**, *138*, 1502-1505.

(16)   Moiseev, I. I.; Stromnova, T. A.; Vargaftig, M. N.; Mazo, G. J.; Kuz'Mina, L. G.; Struchkov, Y. T. New palladium carbonyl clusters: X-ray crystal structure of $[Pd_4(CO)_4(OAc)_4]\cdot(AcOH)_2$. *J. Chem. Soc., Chem. Commun.* **1978**, 27-28.

(17)   Mednikov, E. G.; Eremenko, N. K.; Mikhailov, V. A.; Gubin, S. P.; Slovokhotov, Y. L.; Struchkov, Y. T. New palladium cluster compounds. X-Ray crystal structure of $Pd_{10}(CO)_{12}(P^nBu_3)_6$. *J. Chem. Soc., Chem. Commun.* **1981**, 989-990.

(18)   Mednikov, E. G.; Wittayakun, J.; Dahl, L. F. Synthesis and Stereochemical/Electrochemical Analyses of Cuboctahedral-Based $Pd_{23}(CO)_x(PR_3)_{10}$ Clusters (x = 20 with R_3 = nBu_3, Me_2Ph; x = 20, 21, 22 with R_3 = Et_3): Geometrically Analogous $Pd_{23}(PEt_3)_{10}$ Fragments with Variable Carbonyl Ligations and Resulting Implications. *J. Cluster Sci.* **2005**, *16*, 429-454.

(19)   Mednikov, E. G.; Jewell, M. C.; Dahl, L. F. Nanosized $(\mu_{12}\text{-}Pt)Pd_{164-x}Pt_x(CO)_{72}(PPh_3)_{20}$ (x ≈ 7) Containing Pt-Centered Four-Shell 165-Atom Pd−Pt Core with Unprecedented Intershell Bridging Carbonyl Ligands: Comparative Analysis of Icosahedral Shell-Growth Patterns with Geometrically Related $Pd_{145}(CO)_x(PEt_3)_{30}$ (x ≈ 60) Containing Capped Three-Shell Pd_{145} Core. *J. Am. Chem. Soc.* **2007**, *129*, 11619-11630.

(20)   Teramoto, M.; Iwata, K.; Yamaura, H.; Kurashima, K.; Miyazawa, K.; Kurashige, Y.; Yamamoto, K.; Murahashi, T. Three-Dimensional Sandwich Nanocubes Composed of 13-Atom Palladium Core and Hexakis-Carbocycle Shell. *J. Am. Chem. Soc.* **2018**, *140*, 12682-12686.

(21)   Murahashi, T.; Fujimoto, M.; Oka, M.-a.; Hashimoto, Y.; Uemura, T.; Tatsumi, Y.; Nakao, Y.; Ikeda, A.; Sakaki, S.; Kurosawa, H. Discrete Sandwich Compounds of Monolayer Palladium Sheets. *Science* **2006**, *313*, 1104-1107.

(22)   Wei, J.; Kahlal, S.; Halet, J.-F.; Saillard, J.-Y. Elucidating the Electronic Structure of the Ligated Cuboctahedral Palladium Cluster $[Pd_{13}(\mu_4\text{-}C_7H_7)_6]^{2+}$. *J. Cluster Sci.* **2019**, *30*, 1227–1233.

(23)   Koizumi, T.-a.; Tanaka, K.; Tsuchido, Y.; Tanabe, M.; Ide, T.; Osakada, K. Bimolecular fusion of $[Pd_3(\mu\text{-}CN\text{-}C_6H_3Me_2\text{-}2,6)_3(CN\text{-}C_6H_3Me_2\text{-}2,6)_3]$ induced by Ph_2GeH_2: formation of the redox-active Pd_6Ge_2 complex. *Dalton Trans.* **2019**, *48*, 7541-7545.

(24)   Sunada, Y.; Haige, R.; Otsuka, K.; Kyushin, S.; Nagashima, H. A ladder polysilane as a template for folding palladium nanosheets. *Nat. Commun.* **2013**, *4*, 2014.

(25)   Chen, Y.; Sunada, Y.; Nagashima, H.; Sakaki, S. Theoretical Study of $Pd_{11}Si_6$ Nanosheet Compounds Including Seven-Coordinated Si Species and Its Ge Analogues. *Chem. Eur. J.* **2016**, *22*, 1076-1087.

(26)   Shimamoto, K.; Sunada, Y. Dimensionality Expansion of a Butterfly Shaped Pd_4 Framework: Constructing Edge-Sharing Pd_6 Tetrahedra. *Chem. Eur. J.* **2019**, *25*, 3761-3765.

(27)   Dart, J. W.; Lloyd, M. K.; Mason, R.; McCleverty, J. A.; Williams, J. Properties of isocyanide ligands in metal complexes. Characterisation and voltammetric properties of bis(tertiary phosphine)tris(iso-nitrile)cobalt(I) complexes. *J. Chem. Soc., Dalton Trans.* **1973**, 1747-1751.

(28)   Bharatam, P. V.; Moudgil, R.; Kaur, D. Lewis Donor and Acceptor Interactions of Silylenes: A Theoretical Study. *Organometallics* **2002**, *21*, 3683-3690.

(29)   Parvin, N.; Pal, S.; Echeverría, J.; Alvarez, S.; Khan, S. Taming a monomeric $[Cu(\eta^6\text{-}C_6H_6)]^+$ complex with silylene. *Chem. Sci.* **2018**, *9*, 4333-4337.

(30)   Lewis, R. A.; George, S. P.; Chapovetsky, A.; Wu, G.; Figueroa, J. S.; Hayton, T. W. Synthesis of a cobalt(IV) ketimide with a squashed tetrahedral geometry. *Chem. Commun.* **2013**, *49*, 2888-2890.

(31)   Damon, P. L.; Liss, C. J.; Lewis, R. A.; Morochnik, S.; Szpunar, D. E.; Telser, J.; Hayton, T. W. Quantifying the Electron Donor and Acceptor Abilities of the Ketimide Ligands in $M(N{=}C^tBu_2)_4$ (M = V, Nb, Ta). *Inorg. Chem.* **2015**, *54*, 10081-10095.

(32)   Lewis, R. A.; Morochnik, S.; Chapovetsky, A.; Wu, G.; Hayton, T. W. Synthesis and Characterization of [M$_2$(N=C^{t}Bu$_2$)$_5$]$^-$ (M=Mn, Fe, Co): Metal Ketimide Complexes with Strong Metal–Metal Interactions. *Angew. Chem. Int. Ed.* **2012**, *51*, 12772-12775.

(33)   Lewis, R. A.; Wu, G.; Hayton, T. W. Synthesis and Characterization of an Iron(IV) Ketimide Complex. *J. Am. Chem. Soc.* **2010**, *132*, 12814-12816.

(34)   Lewis, R. A.; Wu, G.; Hayton, T. W. Stabilizing High-Valent Metal Ions with a Ketimide Ligand Set: Synthesis of Mn(N=C^{t}Bu$_2$)$_4$. *Inorg. Chem.* **2011**, *50*, 4660-4668.

(35)   Lewis, R. A.; Smiles, D. E.; Darmon, J. M.; Stieber, S. C. E.; Wu, G.; Hayton, T. W. Reactivity and Mössbauer Spectroscopic Characterization of an Fe(IV) Ketimide Complex and Reinvestigation of an Fe(IV) Norbornyl Complex. *Inorg. Chem.* **2013**, *52*, 8218-8227.

(36)   Soriaga, R. A. D.; Nguyen, J. M.; Albright, T. A.; Hoffman, D. M. Diamagnetic Group 6 Tetrakis(di-tert-butylketimido)metal(IV) Complexes. *J. Am. Chem. Soc.* **2010**, *132*, 18014-18016.

(37)   Ferreira, M. J.; Matos, I.; Ascenso, J. R.; Duarte, M. T.; Marques, M. M.; Wilson, C.; Martins, A. M. Alkylation, Cation Formation, and Insertion Reactions in Titanium Tris(ketimide) Complexes. *Organometallics* **2007**, *26*, 119-127.

(38)   Ferreira, M. J.; Martins, A. M. Group 4 ketimide complexes: Synthesis, reactivity and catalytic applications. *Coord. Chem. Rev.* **2006**, *250*, 118-132.

(39)   Martins, A. M.; Marques, M. M.; Ascenso, J. R.; Dias, A. R.; Duarte, M. T.; Fernandes, A. C.; Fernandes, S.; Ferreira, M. J.; Matos, I.; Conceição Oliveira, M.; Rodrigues, S. S.; Wilson, C. Titanium and zirconium ketimide complexes: synthesis and ethylene polymerisation catalysis. *J. Organomet. Chem.* **2005**, *690*, 874-884.

(40)   Nomura, K.; Yamada, J.; Wang, W.; Liu, J. Effect of ketimide ligand for ethylene polymerization and ethylene/norbornene copolymerization catalyzed by (cyclopentadienyl)(ketimide)titanium complexes–MAO catalyst systems: Structural analysis for Cp∗TiCl$_2$(NCPh$_2$). *J. Organomet. Chem.* **2007**, *692*, 4675-4682.

(41)   Zhang, S.; Piers, W. E.; Gao, X.; Parvez, M. The Mechanism of Methane Elimination in B(C$_6$F$_5$)$_3$-Initiated Monocyclopentadienyl-Ketimide Titanium and Related Olefin Polymerization Catalysts. *J. Am. Chem. Soc.* **2000**, *122*, 5499-5509.

(42)   Bakhoda, A.; Jiang, Q.; Bertke, J. A.; Cundari, T. R.; Warren, T. H. Elusive Terminal Copper Arylnitrene Intermediates. *Angew. Chem. Int. Ed.* **2017**, *56*, 6426-6430.

(43)   Singh, M. K.; Kar, N. K.; Lal, R. A. Synthesis and structural characterization of manganese(III, IV) and ruthenium(III) complexes derived from 2-hydroxy-1-naphthaldehydebenzoylhydrazone. *J. Coord. Chem.* **2009**, *62*, 1677 - 1689.

(44)   Hong, W. P.; Iosub, A. V.; Stahl, S. S. Pd-Catalyzed Semmler–Wolff Reactions for the Conversion of Substituted Cyclohexenone Oximes to Primary Anilines. *J. Am. Chem. Soc.* **2013**, *135*, 13664-13667.

(45)   Cook, A. W.; Hrobárik, P.; Damon, P. L.; Najera, D.; Horváth, B.; Wu, G.; Hayton, T. W. Synthesis and Characterization of a Linear, Two-Coordinate Pt(II) Ketimide Complex. *Inorg. Chem.* **2019**, *58*, 15927–15935.

(46)   Murahashi, T.; Kurosawa, H. Organopalladium complexes containing palladium-palladium bonds. *Coor. Chem. Rev.* **2002**, *231*, 207-228.

(47)   Tan, Y.; Hartwig, J. F. Palladium-Catalyzed Amination of Aromatic C−H Bonds with Oxime Esters. *J. Am. Chem. Soc.* **2010**, *132*, 3676-3677.

(48)   Hanley, P. S.; Marković, D.; Hartwig, J. F. Intermolecular Insertion of Ethylene and Octene into a Palladium−Amide Bond. Spectroscopic Evidence for an Ethylene Amido Intermediate. *J. Am. Chem. Soc.* **2010**, *132*, 6302-6303.

(49)   Villanueva, L. A.; Abboud, K. A.; Boncella, J. M. Synthesis, Characterization, and Crystal Structures of Monomeric and Dimeric Palladium(II) Amide Complexes. *Organometallics* **1994**, *13*, 3921-3931.

(50)   Tanabe, M.; Yumoto, R.; Yamada, T.; Fukuta, T.; Hoshino, T.; Osakada, K.; Tanase, T. Planar $PtPd_3$ Complexes Stabilized by Three Bridging Silylene Ligands. *Chem. Eur. J.* **2017**, *23*, 1386-1392.

(51)   Garçon, M.; Bakewell, C.; Sackman, G. A.; White, A. J. P.; Cooper, R. I.; Edwards, A. J.; Crimmin, M. R. A hexagonal planar transition-metal complex. *Nature* **2019**, *574*, 390-393.

(52)   Ahlrichs, R.; Fenske, D.; Oesen, H.; Schneider, U. Synthesis and Structure of $[Ni(P^tBu_6)]$ and $[Ni_5(P^tBu_6)(CO)_5]$ and Calculations on the Electronic Structure of $[Ni(P^tBu_6)]$ and $(PR)_6$, R = ^tBu, Me. *Angew. Chem. Int. Ed.* **1992**, *31*, 323-326.

(53)   Kong, G.; Harakas, G. N.; Whittlesey, B. R. An Unusual Transition Metal Cluster Containing a Seven Metal Atom Plane. Syntheses and Crystal Structures of $[Mn][Mn_7(THF)_6(CO)_{12}]_2$, $Mn_3(THF)_2(CO)_{10}$, and $[Mn(THF)_6][Mn(CO)_5]_2$. *J. Am. Chem. Soc.* **1995**, *117*, 3502-3509.

(54)   Doyle, G.; Eriksen, K. A.; Van Engen, D. Mixed copper/iron clusters. The preparation and structure of the large planar cluster anions, $Cu_3Fe_3(CO)_{12}{}^{3-}$ and $Cu_5Fe_4(CO)_{16}{}^{3-}$. *J. Am. Chem. Soc.* **1986**, *108*, 445-451.

(55)   Albano, V. G.; Azzaroni, F.; Iapalucci, M. C.; Longoni, G.; Monari, M.; Mulley, S.; Proserpio, D. M.; Sironi, A. Synthesis, Chemical Characterization, and Bonding Analysis of the $[Ag\{Fe(CO)_4\}_2]^{3-}$, $[Ag_4\{\mu_2-Fe(CO)_4\}_4]^{4-}$, and $[Ag_5\{\mu_2-Fe(CO)_4\}_2\{\mu_3-Fe(CO)_4\}_2]^{3-}$ Cluster Anions. X-ray Structural Determination of$[NMe_3CH_2Ph]_4[Ag_4Fe_4(CO)_{16}]$ and $[NEt_4]_3[Ag_5Fe_4(CO)_{16}]$. *Inorg. Chem.* **1994**, *33*, 5320-5328.

(56)   Ohki, Y.; Shimizu, Y.; Araake, R.; Tada, M.; Sameera, W. M. C.; Ito, J.-I.; Nishiyama, H. $Co_6H_8(P^iPr_3)_6$: A Cobalt Octahedron with Face-Capping Hydrides. *Angew. Chem. Int. Ed.* **2016**, *55*, 15821-15825.

(57)   Brayshaw, S. K.; Green, J. C.; Edge, R.; McInnes, E. J. L.; Raithby, P. R.; Warren, J. E.; Weller, A. S. $[Rh_7(P^iPr_3)_6H_{18}][BArF_4]_2$: A Molecular Rh(111) Surface Decorated with 18 Hydrogen Atoms. *Angew. Chem. Int. Ed.* **2007**, *46*, 7844-7848.

(58)   Adams, R. D.; Pearl, W. C.; Wong, Y. O.; Zhang, Q.; Hall, M. B.; Walensky, J. R. Tetrarhena-heterocycle from the Palladium-Catalyzed Dimerization of $Re_2(CO)_8(\mu-SbPh_2)(\mu-H)$ Exhibits an Unusual Host–Guest Behavior. *J. Am. Chem. Soc.* **2011**, *133*, 12994-12997.

(59)   Soriaga, R. A. D.; Javed, S.; Hoffman, D. M. Synthesis of Copper(I) Complexes with Ketimide and Hydrazide Ligands. *J. Cluster Sci.* **2010**, *21*, 567-575.

(60)   Yuan, X.; Sun, C.; Li, X.; Malola, S.; Teo, B. K.; Häkkinen, H.; Zheng, L.-S.; Zheng, N. Combinatorial Identification of Hydrides in a Ligated Ag_{40} Nanocluster with Noncompact Metal Core. *J. Am. Chem. Soc.* **2019**, *141*, 11905-11911.

(61)   Chai, J.; Yang, S.; Lv, Y.; Chen, T.; Wang, S.; Yu, H.; Zhu, M. A Unique Pair: Ag_{40} and Ag_{46} Nanoclusters with the Same Surface but Different Cores for Structure–Property Correlation. *J. Am. Chem. Soc.* **2018**, *140*, 15582-15585.

(62)   Jusélius, J.; Sundholm, D.; Gauss, J. Calculation of current densities using gauge-including atomic orbitals. *J. Chem. Phys.* **2004**, *121*, 3952-3963.

(63)   Sundholm, D.; Fliegl, H.; Berger, R. J. F. Calculations of magnetically induced current densities: theory and applications. *WIREs Comput. Mol. Sci.* **2016**, *6*, 639-678.

(64)   Blanchard, S.; Fensterbank, L.; Gontard, G.; Lacote, E.; Maestri, G.; Malacria, M. Synthesis of Triangular Tripalladium Cations as Noble-Metal Analogues of the Cyclopropenyl Cation. *Angew. Chem. Int. Ed.* **2014**, *53*, 1987-1991.

(65)   Huang, X.; Zhai, H. J.; Kiran, B.; Wang, L. S. Observation of d-orbital aromaticity. *Angew. Chem. Int. Ed.* **2005**, *44*, 7251-7254.

(66)   Fliegl, H.; Lehtonen, O.; Lin, Y.-C.; Patzschke, M.; Sundholm, D. Theoretical investigation of photoelectron spectra and magnetically induced current densities in ring-shaped transition-metal oxides. *Theor. Chem. Acc.* **2011**, *129*, 701-713.

(67)   Mann, B. E.; Musco, A. Phosphorus-31 nuclear magnetic resonance spectroscopic characterisation of tertiary phosphine palladium(0) complexes: evidence for 14-electron complexes in solution. *J. Chem. Soc., Dalton Trans.* **1975**, 1673-1677.

(68)   Tolman, C. A.; Seidel, W. C.; Gerlach, D. H. Triarylphosphine and ethylene complexes of zerovalent nickel, palladium, and platinum. *J. Am. Chem. Soc.* **1972**, *94*, 2669-2676.

(69)   Johansson Seechurn, C. C. C.; Kitching, M. O.; Colacot, T. J.; Snieckus, V. Palladium-Catalyzed Cross-Coupling: A Historical Contextual Perspective to the 2010 Nobel Prize. **2012**, *51*, 5062-5085.

(70)   Roy, D.; Uozumi, Y. Recent Advances in Palladium-Catalyzed Cross-Coupling Reactions at ppm to ppb Molar Catalyst Loadings. *Adv. Synth. Catal.* **2018**, *360*, 602-625.

(71)   Biffis, A.; Centomo, P.; Del Zotto, A.; Zecca, M. Pd Metal Catalysts for Cross-Couplings and Related Reactions in the 21st Century: A Critical Review. *Chem. Rev.* **2018**, *118*, 2249-2295.

(72)   Baumann, C. G.; De Ornellas, S.; Reeds, J. P.; Storr, T. E.; Williams, T. J.; Fairlamb, I. J. S. Formation and propagation of well-defined Pd nanoparticles (PdNPs) during C–H bond functionalization of heteroarenes: are nanoparticles a moribund form of Pd or an active catalytic species? *Tetrahedron* **2014**, *70*, 6174-6187.

(73)   Clegg, W.; Snaith, R.; Shearer, H. M. M.; Wade, K.; Whitehead, G. Azomethine derivatives. Part 20. Crystal and molecular structures of the lithioketimine [{Li(N=CBu^{t2})}$_6$] and lithioguanidine [{Li[N=C(NMe$_2$)$_2$]}$_6$]; electron-deficient bridging of Li$_3$ triangles by methyleneamino-nitrogen atoms. *J. Chem. Soc., Dalton Trans.* **1983**, 1309-1317.

(74)   Anderson, G. K.; Minren, L. Reagents for Transition Metal Complex and Organometallic Syntheses. *Inorg. Synth.* **1990**, *28*, 61.

SYNOPSIS
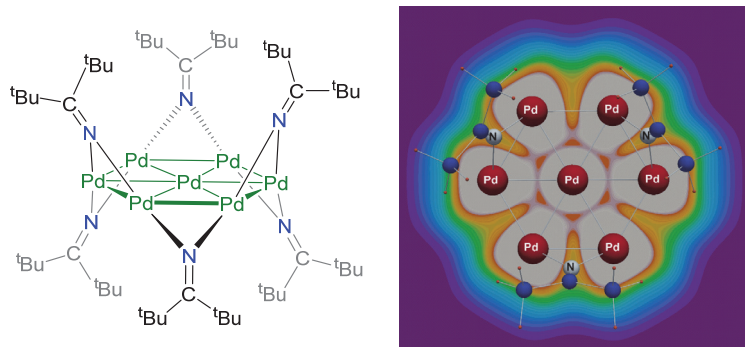
Reaction of $PdCl_2(PhCN)_2$ with $Li(N=C^tBu_2)$ results in formation of the Pd_7 nanosheet, $Pd_7(N=C^tBu_2)_6$, demonstrating that ketimides are effective at stabilizing low-valent group 10 nanoclusters.